Quantifying variability of Large Eddy Simulations of very large wind farms

2015 J. Phys.: Conf. Ser. 625 012027

(http://iopscience.iop.org/1742-6596/625/1/012027)

Journal of Physics: Conference Series **625** (2015) 012027 doi:10.1088/1742-6596/625/1/012027

Quantifying variability of Large Eddy Simulations of very large wind farms.

S J Andersen[1a], B Witha[2], S-P Breton[3], J N Sørensen[1,3], R F Mikkelsen[1], and S Ivanell[3]

[1] DTU Wind Energy, Technical University of Denmark, 2800 Lyngby, Denmark.
[2] ForWind - Center for Wind Energy Research, Carl von Ossietzky University Oldenburg, Ammerländer Heerstr. 136, 26131 Oldenburg, Germany.
[3] Uppsala University, Dep. of Earth Sciences, Campus Gotland, Visby, Sweden.

E-mail: [a] sjan@dtu.dk

Abstract. Large Eddy Simulations are inherently dynamic as the largest scales are resolved and the smallest scales are modeled temporally. This raises challenges for simulations including very large scales such as atmospheric flows, which require very long simulation times. Simple averages fail at capturing these dynamics and potentially yield misleading interpretations concerning the capabilities of different models when tested in blind tests or in benchmarking exercises such as Wakebench, where results from different flow models are compared. This article will present results from very large wind farm simulations using Actuator Disc (AD) and Line (AL) models for two different turbine spacings with turbulent inflow. The results of each numerical flow model include a certain variability, and it will be examined if different models result in comparable probability distributions.

1. Introduction

The state-of-the-art in numerical simulations of wind turbines and wind farms consists of Large Eddy Simulations (LES) combined with Actuator Disc (AD) or Actuator Line (AL) methods to model the flow behind and between wind turbines. LES are inherently dynamic as the largest scales are resolved and the smallest scales are modeled temporally. This yields important advantages but also raises challenges in comparing results from otherwise comparable simulations. Simple averages do not capture the dynamics. Particularly, too short averaging times which do not filter out large turbulent structures, a common feature in the atmospheric boundary layer, may yield misleading interpretations concerning the capabilities of different models. This provides a challenge when models are tested and compared with measurements, benchmarking exercises or in blind tests such as the Bolund Experiment [1]. LES require long simulation times before statistical convergence is achieved, see e.g. Andersen [2] who examined the statistical convergence of the turbulent quantities in infinitely large wind farms. This is resource consuming and the required convergence time might differ for different models and setups. Yet, it is also standard procedure in atmospheric and wind energy related measurements to report 10 min averages.

The present article aims at examining the variability from different model simulations performed by different users in order to explore how the variability can be presented and compared best. Furthermore, the analysis will investigate if the variability can be exploited

to provide valuable insights in terms of overall confidence in model results as well as in potentially building a bridge to the natural variability found in measurements, where results and measurements are often filtered to compare well.

The results presented have been derived from a benchmarking exercise of the IEA Wind Task 31: Wakebench[1]. In that benchmark very large wind farms are to be simulated to determine if and when an asymptotic wake state as in an infinite wind farm is reached. A range of different methods to simulate the turbulent flow and model the effect of the wind turbines are used by the participants. Hence, the aim of this article is to present graphical methods for comparing and evaluating the temporal and spatial variability resulting from the different approaches.

This article will present results from very large wind farm simulations using AL and AD models in EllipSys3D [3], [4] from Technical University of Denmark (DTU) and Uppsala University (UU) and PALM [5], [6] from ForWind (FW) for different turbine spacings. Each numerical flow model produces a spatially and temporally variable flow, and it will be examined if different models result in comparable probability distributions.

2. Methodology

This section gives a brief introduction to the difference in methodology applied by the different participants but refers to other papers for detailed information on the theoretical background.

2.1. Numerical Solvers

Results from two different CFD codes are used.

2.1.1. EllipSys3D EllipSys3D is a 3D flow solver developed as a collaboration between DTU (Michelsen [3]) and the former Risø(Sørensen [4]), and has been applied for wind energy research for more than two decades. EllipSys3D solves the discretized incompressible Navier-Stokes equations in general curvilinear coordinates using a block structured finite volume approach. EllipSys3D is formulated in primitive variables (pressure-velocity) in a collocated grid arrangement. Additional details can for instance be found in Mikkelsen [7] and Troldborg [8].

2.1.2. PALM PALM (Parallelized LES Model) is an open source highly parallelized LES model which has been applied for the simulation of a variety of atmospheric and oceanic boundary layers for more than 15 years. PALM solves the filtered, incompressible, non-hydrostatic Navier-Stokes equations under the Boussinesq approximation on an equidistant Cartesian grid. The sub-grid scale turbulence is parameterized by a 1.5th order closure after Deardorff [9]. Further details can be found in Maronga et al. [6]. Recently, it has been adapted by FW for the simulation of wind turbine wakes, see Witha et al. [10].

2.2. Turbine Modeling

2.2.1. EllipSys3D The wind turbines are modeled using either the AL (by DTU) or AD (by UU) method where body forces are distributed along rotating lines or on a disc, respectively, see Mikkelsen [7] and Troldborg et al. [11] as well as Sørensen and Shen [12] for details on the EllipSys3D implementation of the AL and AD. Tabularized airfoil data is used to determine the local blade forces based on the local inflow conditions. In the DTU-AL model, the 2D airfoil data is corrected to account for 3D effects, see e.g. Hansen et al. [13]. Furthermore, the body forces in the DTU implementation are calculated through a full coupling with Flex5, a full aeroelastic code for calculating deflections and loads on wind turbines, see Øye [14] for details on Flex5 and Sørensen et al. [15] for a description of the coupling.

[1] `http://www.ieawind.org/task_31.html`

2.2.2. PALM The PALM implementation contains two different turbine models. The standard Actuator Disc model with uniform force distribution (FW-AD-U) uses an aerodynamic thrust curve and the velocity averaged over the rotor disc together with an axial induction factor to determine the thrust force which is the same all over the rotor plane. The second model is an enhanced AD model with rotation (FW-AD-R) in which local body forces are calculated by means of BEM theory. In contrast to the AL method, the forces are distributed across the rotor plane. Both FW-AD-U and FW-AD-R include tower and nacelle effects modeled by a drag force approach. See Dörenkämper et al. [16] for details of the PALM implementation.

2.2.3. Turbine Controller Three of the four models (DTU-AL, UU-AD and FW-AD-R) include a turbine controller which effectively means that the applied body forces are governed by the inflow conditions, i.e. the turbines are not constantly loaded, but operate as "real turbines". A general description of such controllers can be found in Larsen and Hanson [17] or Hansen et al. [18].

2.2.4. Turbine Data Two different turbines have been used: the NM80 and the NREL 5MW. Both are three bladed horizontal axis wind turbines. The NM80 turbine is proprietary to Vestas Wind Systems A/S, but reference is made to the DAN-AERO MW Experiments, see Madsen et al. [19]. NM80 has a radius $R = 40$ m and is rated to 2.75 MW at a hub height velocity of $U_{hub} = 14$ ms^{-1}. The NREL 5MW has a radius of $R = 63$ m, a hub height of $z_{hub} = 90$ m and is rated to 5 MW at $U_{hub} = 11.4$ ms^{-1}, see Jonkman et al. [20].

Table 1 summarizes the different methods used by the participants.

3. Simulations Setup

The coordinate system used in this work is defined such that x, y and z correspond to the streamwise, crosswise and vertical directions, respectively. The grids used the simulation are equidistant in the horizontal directions. The grid used in the DTU simulation is also vertically uniform whereas the grids used in the FW and UU simulations are stretched in the vertical direction from a height far above the wind farm (FW: 9.5 R, UU: 8 R). Further details of the setup are given in Table 1 and in the text below.

3.1. Atmospheric Boundary Layer and Turbulence

All participants simulated a neutrally stratified atmospheric boundary layer and aimed at obtaining an average streamwise inflow velocity of $U_0 = 8$ ms^{-1} and an average inflow turbulence intensity (TI, streamwise component) of $\sigma_u/U_0 = 15\%$, both at hub height.

3.1.1. EllipSys3D EllipSys3D uses the prescribed boundary layer method (PBL) which utilizes body forces to achieve any arbitrary vertical wind shear profile, see Mikkelsen et al. [21] and Troldborg et al. [22]. A comparison of PBL with a wall model approach was performed by Sarlak et al. [23] which showed that the two approaches yield very comparable vertical profiles of mean streamwise velocity, shear stress, and streamwise velocity fluctuations in the rotor region when modeling large wind farms. The modeling of the ambient turbulence is performed by introducing pregenerated synthetic ambient turbulence. The ambient turbulence is generated using the Mann model, [24]. Turbulence planes are imposed at an axial position of 6 R and 13 R for the DTU and UU simulations, while the first simulated turbine is located at 10 R and 30 R, respectively.

3.1.2. PALM The atmospheric boundary layer is modeled in PALM using a no-slip bottom boundary condition and Monin-Obukhov similarity theory between the surface and the first grid level. Initially, random perturbations are imposed on the velocity fields until atmospheric turbulence has developed in a precursor simulation, which is performed on a smaller domain and with periodic boundary conditions in streamwise and lateral directions. The precursor results are used to initialize the full simulations with non-periodic boundary conditions in the streamwise direction and additionally turbulence recycling was applied, see Maronga et al. [6] for details.

3.2. Wind Farm
A very large wind farm has been simulated, containing 16 turbines in the streamwise direction and an infinite number of turbines in the lateral direction (by applying periodic boundary conditions). Two different streamwise turbine spacings of $S_x = 12\ R$ and $S_x = 20\ R$ have been simulated by all participants (see Table 2). The lateral spacing is $S_y = 20\ R$ for both simulations.

Table 1. Summary of methods and simulations by DTU and FW.

Method	*DTU-AL*	*FW-AD-U*	*FW-AD-R*	*UU-AD*
CFD Solver	EllipSys3D	PALM	PALM	EllipSys3D
Domain Size [R]	$200/320 \times 20 \times 20$	$343/533 \times 38 \times 35$	$343/533 \times 38 \times 35$	$374 \times 20 \times 40$
Equiv. roughness [m]	N/A	1 m	1 m	0.5 m
Turbine	NM80	NREL 5MW	NREL 5MW	NREL 5MW
R	40 m	63 m	63 m	63 m
z_{hub}	80 m	90 m	90 m	90 m
Controller	Yes	No	Yes	Yes
3D effects correction	Yes	No	No	No
Resolution [R]	0.0625	0.127	0.127	0.0781

4. Results and Discussion
All datasets have been interpolated in time to have a sampling rate of 1 Hz and all raw data were post-processed in the same way. The data have been sampled after running the models the equivalent time of at least two flow-throughs in the domain in order to avoid any transients from the simulation startup. Different types of data will be presented: instantaneous data, averages of the entire sampling period (as given in Table 2), as well as 10 min averages. The 10 min averages are computed within the total sampling period by shifting the averaging window by 1 min to get a larger number of samples[2].

4.1. Inflow Conditions
Despite aiming at setting up and simulating exactly the same case, the different methodologies and codes result in different inflows. The temporally averaged streamwise velocity and streamwise TI profiles extracted 1 R upstream the first turbine are shown in Figure 1. TI is here defined as σ_u/U_0. The vertical profiles have been shifted to be aligned at hub height, which is marked by dashed lines. The velocity for the FW simulations is slightly less than for the DTU simulation. At the same time, the vertical shear is larger, which could be attributed

[2] *i.e.* the 10 min averages are not independent in a statistical sense

Table 2. Overview of simulations by DTU and FW with the time periods (from the end of the simulation) used for evaluation.

Method	*DTU-AL*	*FW-AD-U*	*FW-AD-R*	*UU-AD*
$S_x = 12\ R$	60 min	60 min	60 min	30 min
$S_x = 20\ R$	30 min	60 min	60 min	30 min

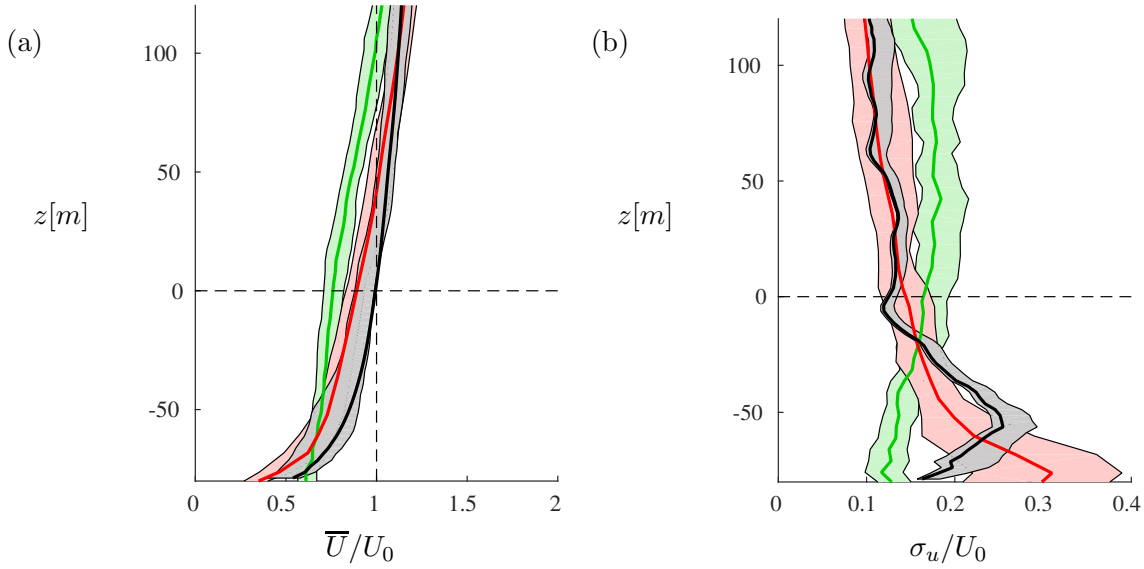

Figure 1. Vertical profiles of a) average streamwise velocity and b) streamwise fluctuations extracted 1 R upstream the first turbine. The profiles are shifted to have hub height at $y = 0$ to enable a direct comparison. Black: DTU-AL. Red: FW-AD-R. Green: UU-AD. The thick lines denote the temporal average over all 10 min averages within the evaluation period given in Table 2. The shaded areas give the maximum and minimum of the 10 min averages.

to the large effective roughness which had to be used in the FW simulations to reach the desired TI. The UU simulation shows a lower velocity than both the FW and DTU simulations, except close to the ground, where it finds itself somewhere between FW and DTU. The lower inflow velocities in the FW and UU simulations can be attributed to a longer induction zone of the first turbine compared to the DTU simulation, so that 1 R upstream, the FW and UU flow is already affected by the first turbine. See section 4.2 for further elaboration. Above hub height, the FW and DTU TI profiles are very similar whereas they differ to some extent below hub height. The UU profile is considerably different from the two others and does not follow the typical shape of atmospheric boundary layer turbulence with increasing turbulence towards the ground. Whereas the TI is higher around and above hub height, it is lower near the ground, compared to the other simulations. The observed differences could be explained by the different approaches used to generate turbulence, which highlights how a direct comparison can be very difficult, when different methods are compared. The turbulence in the DTU simulations is scaled to fit measured turbulence close to the ground, which makes it quite similar to the FW profiles. Such a scaling was not performed in the UU simulations, explaining the differences obtained close to the ground.

4.2. Average Velocities and Turbulent Fluctuations.
The average streamwise velocity at hub height through the wind farm is compared in Figure 2. The data has been averaged over the entire time period given in Table 2. Despite the different inflow conditions, all simulations follow a very comparable pattern, almost sinusoidal, and it is evident how the average streamwise velocity very quickly converges to a constant level between the turbines[3], at least for the DTU and FW simulations. The UU-AD results are less constant and appear to peak around the 11th turbine for $S_x = 12\ R$ and the 8th turbine for $S_x = 20\ R$. Generally, the average streamwise velocity has reached a converged level already at the fourth turbine, after which the streamwise velocity trend does not vary significantly. The dashed lines in Figure 2 indicates the mean of the average streamwise velocity 1 R upstream the turbines after the fourth turbine. The EllipSys3D (DTU and UU) results systematically show higher velocities compared to the results provided by FW for both spacings. This holds especially true for the wake of the first two turbines. The two FW simulations provide very similar results, although there is a tendency of higher amplitude between the "wave crest" and "trough" between each set of turbines with the standard AD-U.

The converged velocity or asymptotic wake deficit is often denoted as the "infinite wind farm" scenario. Several low fidelity models estimate the converged velocity ratio in an "infinite wind farm", e.g. N. O. Jensen [25] and Frandsen et al. [26]. These simple engineering models are independent of rotor details (except the thrust coefficient), the vertical shear and TI of the inflow. Hence, the present simulations could be used to scale the model parameters, similar to what was done by Andersen [27] for infinite wind farm simulations. The converged streamwise velocity extracted 1 R upstream the turbines has been averaged from the fourth to the 16th turbine and plotted with a dashed line in Figure 2 and summarized in Table 3. The converged velocity ratios can be compared to velocity ratios obtained by Andersen [2], who reported $\overline{U}/U_0 = 0.8$ for turbine spacings of $S_x = 20\ R$, where the "infinite wind farm" was achieved by applying cyclic boundary conditions. The simulations used an inflow velocity of 15 ms^{-1}, no added turbulence and a smaller vertical shear, but as seen the converged result is the same. It has to be noted, however, that the internal wind farm boundary layer (IWBL) above the turbines is continuously growing until the last of the 16 simulated turbines. So, although the velocity deficit converges very quickly after three or four turbines (for most cases), a true "infinite wind farm" scenario would require many more turbines. Tests by FW with 50 turbine rows have shown that the IWBL is still (slowly) increasing until the last row.

It is also interesting to note the difference in inflow to the first turbine as previously shown in Figure 1. The difference in inflow velocity at 1 R is here seen to be related to the induction upstream the first turbine. The apparent large difference in Figure 1 merely stems from the steep slope around 1 R. Further upstream the inflow is comparable. The flow at 1 R upstream each turbine is taken as representative of the inflow to each turbine inside the farm. The length of the induction zone in front of each turbine can also be estimated based on the distance from the local maximum velocity in front of each turbine to the turbine itself, i.e. using the fact that the wake velocity is no longer recovering from the latter position due to the adverse pressure gradient from the wind turbines. This simple analysis yields very similar estimates of the induction zone from the different simulations (see Table 3), although it is noteworthy how the length of the induction zone increases from approximately 2 R to 3 R as the spacing between the turbines increases from $S_x = 12\ R$ to $S_x = 20\ R$. This is attributed to the stronger wake recovery for the larger spacing, i.e. the wake is less dominant and hence more sensitive to the influence of the following turbine. A more detailed investigation of the wind evolution within the induction zone has previously been performed by Simley et al. [28].

The streamwise turbulent fluctuations, as shown in Figure 3 are initially higher in the DTU

[3] When speaking of convergence we mean the velocity at the same relative position between each set of turbines, e.g. the values of the relative maxima and minima behind each turbine

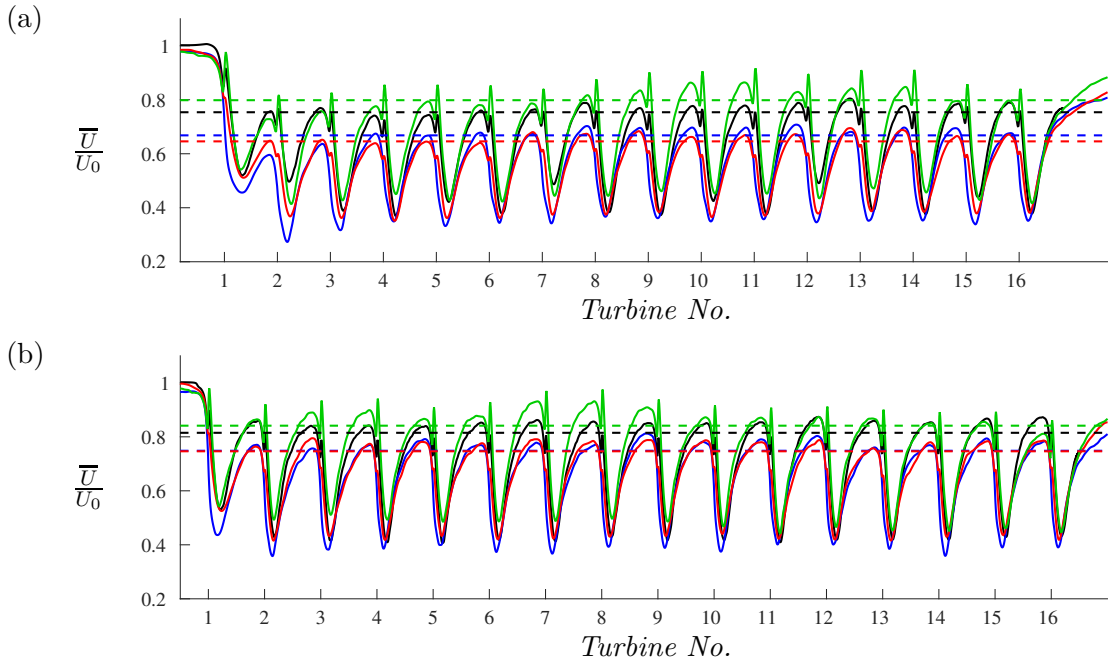

Figure 2. Mean streamwise velocity through the wind farms at hub height for different spacings: a) $S_x = 12\ R$. b) $S_x = 20\ R$. Black: DTU-AL. Blue: FW-AD-U. Red: FW-AD-R. Green: UU-AD.

Table 3. Converged velocity ratios $\overline{U}/U_0$ and length of induction zone Δ_I for very large wind farms for all simulations.

		DTU-AL	*FW-AD-U*	*FW-AD-R*	*UU-AD*
$S_x = 12\ R$	$\overline{U}/U_0$	0.71	0.67	0.65	0.80
	Δ_I	-2.01 R	-2.06 R	-2.20 R	-2.06 R
$S_x = 20\ R$	$\overline{U}/U_0$	0.80	0.75	0.75	0.84
	Δ_I	-3.16 R	-3.10 R	-3.04 R	-3.23 R

and UU simulations, leading to a significantly higher velocity behind the first two turbines, but generally and consistently the streamwise turbulent fluctuations of the FW and UU simulations exceed those found in the DTU simulations after the third turbine. This is particularly the case for the FW-AD-R with higher TI between the turbines, but lower in the rotor plane compared with the same simulations with AD-U. The higher TI in the FW simulations could possibly be explained by the substantially higher TI in the lower rotor plane (see Figure 1) which is lifted up by mixing and rotation of the wake. This explanation is however not supported by the fact that the UU simulation, which features a very low TI below hub height, shows a similarly high TI as the FW-AD-R simulation in Fig. 3. Furthermore, a consistently higher turbulence intensity should intuitively result in greater wake recovery, hence increasing streamwise velocities further into the farm. However, this is not the case as the velocity maxima between the turbines are nearly constant, see Figure 2.

So far only long-time averages have been considered. For a better assessment of the dynamics and variability of the different LES, distributions of instantaneous velocity and wind direction

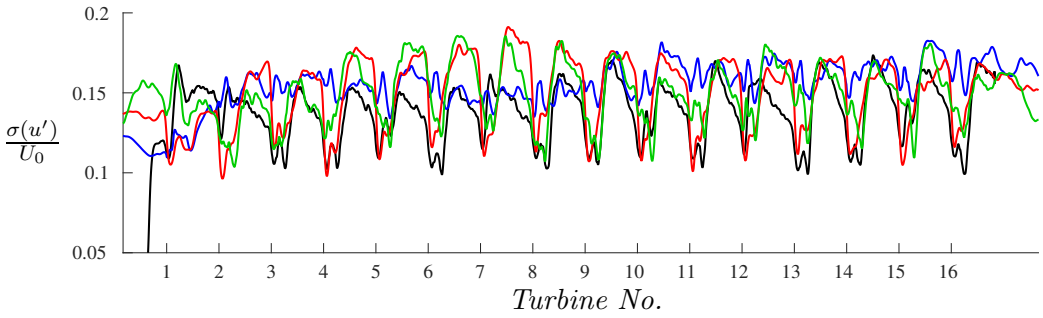

Figure 3. Mean streamwise TI through the wind farms at hub height for $S_x = 12\ R$. Black: DTU-AL. Blue: FW-AD-U. Red: FW-AD-R. Green: UU-AD.

will be investigated in the following section.

4.3. Velocity Distributions

Figure 4 shows box plots of the instantaneous (1 Hz) streamwise velocities extracted 1 R upstream of each of the turbines. A box plot is a simple way of depicting the variability of a data and is drawn by horizontal lines defining the first quartile q_1, median, and third quartile q_3, as well as vertical lines. The line extends to $q_3 \pm w(q_3 - q_1)$, where $w = 1.5$. This would correspond to $\pm 2.7\sigma$ equivalent to 99.3% coverage if the data is normally distributed. Finally, any outliers outside this extent are marked by crosses.

As expected, the median level follows the same trend as the long term averages. Generally, the variability is comparable, though slightly smaller for the DTU results, seen by comparing the box extent between the first and third quartile. The first and third quartile span a maximum variability of 21.5%, 24.4%, 25.0%, and 27.2% on the instantaneous axial velocity extracted from the simulations by DTU-AL, FW-AD-U, FW-AD-R, and UU-AD, respectively. For the larger turbine spacing, the variability is slightly reduced to 18.7%, 22.2%, 24.7%, and 23.1% for the four datasets. There are also more outliers in the UU results, which again indicates a larger variability. The outliers constitute approximately 0.33%, 0.85%, 1.45%, and 2.92% of the instantaneous axial velocities for $S_x = 12\ R$ from DTU-AL, FW-AD-U, FW-AD-R and UU-AD, respectively. Similar values are obtained for $S_x = 20\ R$.

The averages shown for the streamwise velocity and fluctuations are averaged over long periods (30-60 min). Within wind energy and atmospheric studies, it is standard to report 10 min averages, which is also often set as criteria for blind test and benchmarks. Hence, Figure 5 depicts box plots based on 10 min averages of the streamwise velocity. Averaging reduces the average span between the first and third quartile to 6.2%, 9.4%, 9.1%, and 5.0% for the four datasets for $S_x = 12\ R$. Interestingly, the variability is reduced relatively more in the UU-AD results compared to the other simulations. Similar variability is seen for $S_x = 20\ R$, but left out for brevity.

4.4. Directional Variation

The variability is not only temporal, but also spatial or directional. Figure 6 shows the distributions of wind direction based on the instantaneous horizontal velocity components for the first and the ninth turbine with spacing $S_x = 12\ R$. The ninth turbine is shown, because the box plots are most similar for this particular turbine. The directional variability of the inflow to the first turbine is very similar and very symmetric about 270° for the DTU and FW-AD-U results. The case FW-AD-R is not as symmetric. The wind is from $270° \pm 2.5°$ in 30% of the time in all these three simulations, and from the adjacent sectors of $265 \pm 2.5°$ and $275 \pm 2.5°$

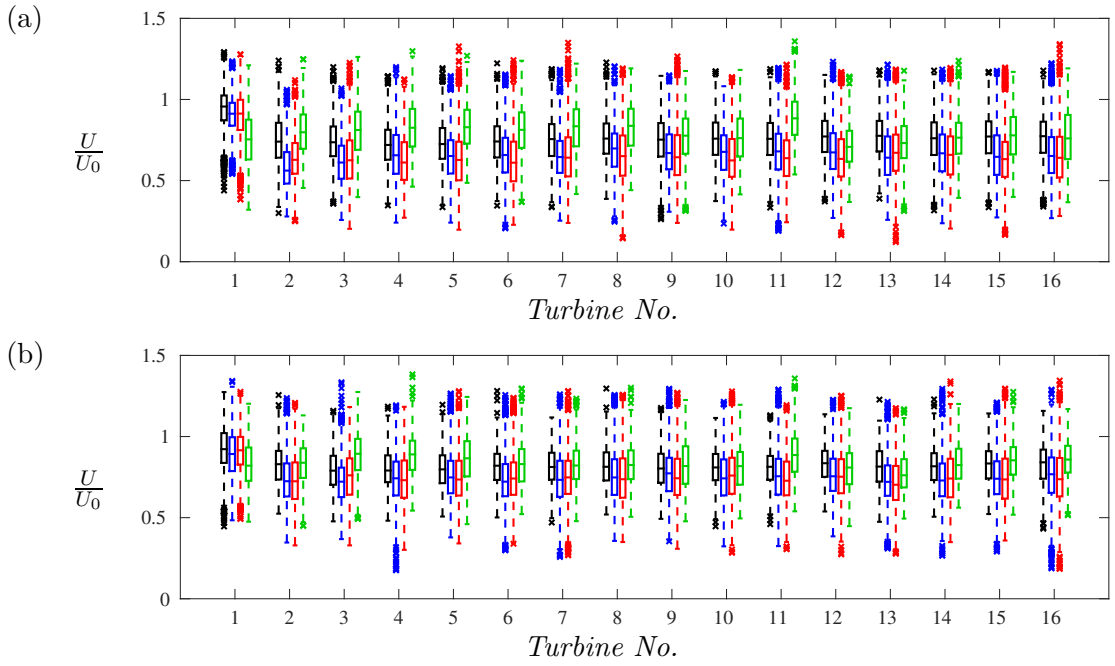

Figure 4. Box plots comparing instantaneous (1 Hz) streamwise velocity distributions extracted 1 R upstream of each of the turbines. a) $S_x = 12\ R$. b) $S_x = 20\ R$. Black: DTU-AL. Blue: FW-AD-U. Red: FW-AD-R. Green: UU-AD.

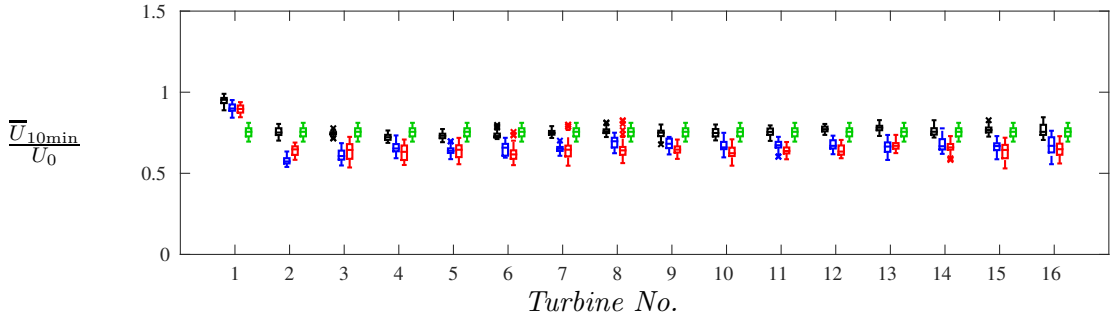

Figure 5. Box plots distributions of 10 min averages of streamwise velocities extracted 1 R upstream of each of the turbines for $S_x = 12\ R$. Black: DTU-AL. Blue: FW-AD-U. Red: FW-AD-R. Green: UU-AD.

approximately 10% of the time, except for FW-AD-R with slight bias to higher degrees. In this case, the inflow is not exactly parallel to the streamwise direction, because the FW simulations include the Coriolis force, thus the wind is turning with height. It is not trivial to find the suitable prescribed wind speed to obtain a flow exactly aligned with the x-axis at hub height. Methods have been proposed to adjust the geostrophic wind during the simulation to obtain an aligned flow (e.g. by Sescu and Meneveau [29]) but not been implemented in the PALM code, so far. Apart from the very slight differences in wind direction, not modeling the Coriolis force in the DTU and UU simulations is not expected to affect the presented results. As previously seen, the DTU results show a slightly higher velocity. The UU-AD results are seen to be quite different from the three other cases, as the directional variability around the streamwise direction is much larger upstream of the first turbine. This is stems from the direct application of the unscaled Mann turbulence. The DTU simulations also apply Mann turbulence, but this has been scaled

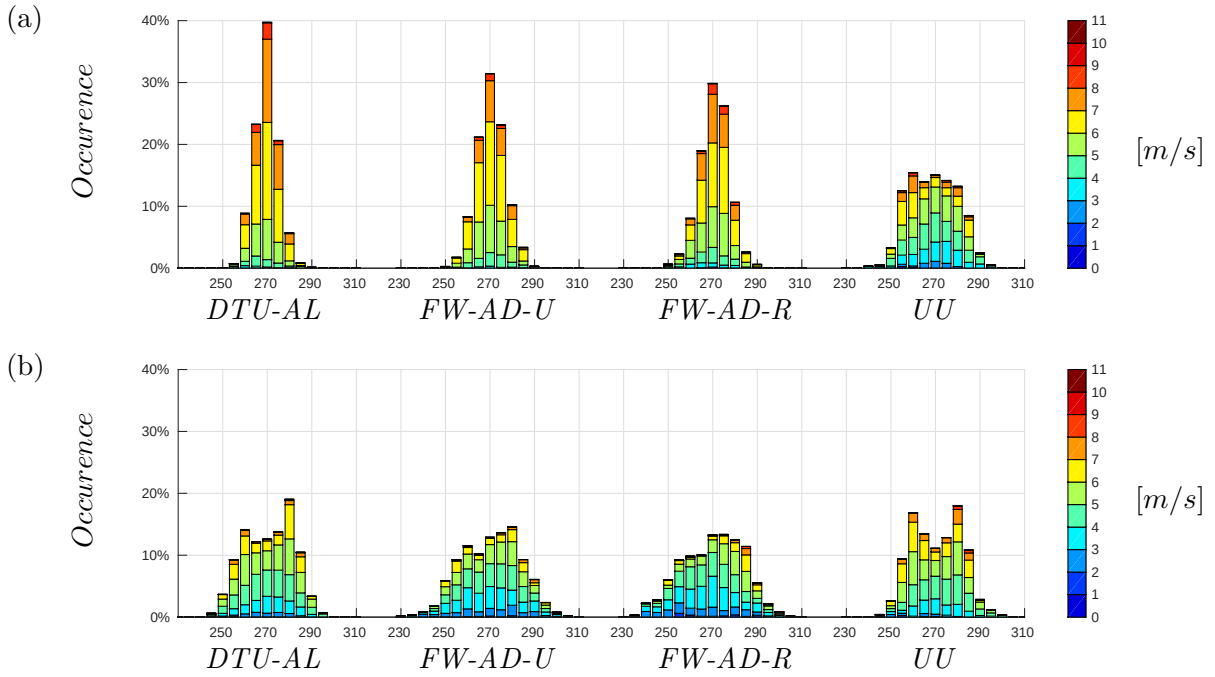

Figure 6. Directional variability of horizontal velocities (U and V components) extracted 1 R upstream the first and ninth turbine for $S_x = 12\ R$. 270 degrees corresponds to completely aligned inflow.

to fit measure turbulence statistics as mentioned in 4.1, which yields a decrease of the spanwise fluctuations close to the ground.

The directional variability for the ninth turbine is quite comparable between the four simulations. However, the distribution is considerably wider than for the first turbine ($\approx 270° \pm 30°$) and it is noteworthy how the dominant direction is shifted towards $280° \pm 2.5°$ for the DTU and FW simulations. The UU simulation also has a peak here, but is more symmetric with a second minor peak at $260° \pm 2.5°$. Such a minor peak is also present in the DTU results, although the shifted distribution is more comparable to the FW results.

This change in dominant direction is not as clear for the larger spacing $S_x = 20\ R$ (not shown).

5. Conclusions

A total of eight datasets derived from LES simulations of very large wind farms with two different turbine spacings have been compared using four different model setups. Despite differences in model setup and inflow conditions, the simulations yielded a number of comparable results. At least three of the four simulations showed that the "infinitely large wind farm" in terms of average streamwise velocity at hub height (at the same relative position between each set of turbines) was achieved by the fourth turbine, although the simulations resulted in slightly different velocity levels. The streamwise fluctuations were comparable, though one simulation showed slightly lower values compared to the other simulations. The temporal variability of streamwise velocity, both instantaneous and 10 min averages, was also very comparable. However, the variability analysis showed that there could still be significant differences between individual 10 min averages from the same simulation despite averaging. Hence, longer simulation times and longer averages are required to enable reporting such variability for comparing in e.g. benchmarks. Finally, the directional variability was examined through wind distribution plots,

which were also equivalent in most cases despite the model differences.

Examining the variability of LES simulations could bridge the gap between measurements and simulations within very large wind farms. As the results show both temporal and directional variability, the variability could potentially be compared with the variability found in measurements, whereas the variability is usually filtered out in order to compare measurements and simulations.

Acknowledgments

The work has been carried out with the support of the Danish Council for Strategic Research for the project *Center for Computational Wind Turbine Aerodynamics and Atmospheric Turbulence* (grant 2104-09-067216/DSF) (COMWIND: http://www.comwind.org), in the framework of the project *Parallelrechner-Cluster für CFD und WEA-Modellierung* funded by the German Federal Ministry for Economic Affairs and Energy (FKZ: 0325220), as part of the EUROTECH Wind project, and with support of the Nordic Consortium on Optimization and Control of Wind Farms funded by the Swedish Energy Agency. Computer time was granted by the Swedish National Infrastructure for Computing (SNIC) and by the North German Supercomputing Alliance (HLRN). Furthermore, the proprietary data for Vestas' NM80 turbine has been used.

References

[1] Bechmann A, Sørensen N, Berg J, Mann J and Réthoré P 2011 The Bolund Experiment. Part II: Blind Comparison of Microscale Flow Models *Boundary-Layer Meteorol.* **141** 245–271 ISSN 0006-8314

[2] Andersen S J 2013 *Simulation and Prediction of Wakes and Wake Interaction in Wind Farms* Ph.D. thesis Technical University of Denmark, Wind Energy.

[3] Michelsen J A 1992 Basis3D – a Platform for Development of Multiblock PDE Solvers Tech. rep. Danmarks Tekniske Universitet

[4] Sørensen N N 1995 *General Purpose Flow Solver Applied to Flow over Hills* Ph.D. thesis Technical University of Denmark

[5] Raasch S and Schröter M 2001 PALM - A large-eddy simulation model performing on massively parallel computers *Meteorol. Z.* **10** 363–372

[6] Maronga B, Gryschka M, Heinze R, Hoffmann F, Kanani-Sühring F, Keck M, Ketelsen K, Letzel M O, Sühring M and Raasch S 2015 The Parallelized Large-Eddy Simulation Model (PALM) version 4.0 for atmospheric and oceanic flows: model formulation, recent developments, and future perspectives *Geosci. Model Dev. Discuss.* **8** 1539–1637

[7] Mikkelsen R 2003 *Actuator Disc Methods Applied to Wind Turbines* Ph.D. thesis Technical University of Denmark, Mek dept

[8] Troldborg N 2008 *Actuator Line Modeling of Wind Turbine Wakes* Ph.D. thesis DTU Mechanical Engineering, Technical University of Denmark, DTU, DK-2800 Kgs. Lyngby, Denmark Denmark

[9] Deardorff J 1980 Stratocumulus-capped mixed layers derived from a three-dimensional model *Boundary-Layer Meteorol.* **18** 495–527

[10] Witha B, Steinfeld G and Heinemann D 2014 *Wind Energy - Impact of Turbulence* Research Topics in Wind Energy 2 ed Hölling M, Peinke J and Ivanell S (Springer Berlin Heidelberg) pp 175–181

[11] Troldborg N, Gaunaa M and Mikkelsen R 2010 Actuator Disk Simulations on Influence of Wind Shear on Power Production of Wind Turbines *Proceedings of the V European Conference on Computational Fluid Dynamics, 14-17 June 2010, Lisbon, Portugal*

[12] Sørensen J N and Shen W Z 2002 Numerical modelling of Wind Turbine Wakes *J. Fluids Eng.* **124** 393–399

[13] Hansen M O L, Sørensen J N, Voutsinas S, Sørensen N and Madsen 2006 State of the art in wind turbine aerodynamics and aeroelasticity *Prog. Aerosp. Sci.* **42** 285–330

[14] Øye S 11-12 April 1996 Flex4 simulation of wind turbine dynamics (Lyngby, Denmark: Danmarks Tekniske Universitet) pp 71–76

[15] Sørensen J, Mikkelsen R, Henningson D, Ivanell S, Sarmast S and Andersen S 2015 Simulation of wind turbine wakes using the actuator line technique *Phil. Trans. R. Soc. A* **373** ISSN 1364-503X

[16] Dörenkämper M, Witha B, Steinfeld G, Heinemann D and Kühn M 2015 The impact of stable atmospheric boundary layers on wind-turbine wakes within offshore wind farms *J. Wind Eng. Ind. Aerodyn.* Accepted for publication

[17] Larsen T and Hanson T 2007 A method to avoid negative damped low frequent tower vibrations for a floating, pitch controlled wind turbine *J. Phys.: Conf. Ser.* **75** 11
[18] Hansen M H, Hansen A, Larsen T J, Oye S, Sorensen P and Fuglsang P 2005 *Control design for a pitch-regulated, variable speed wind turbine* Denmark. Forskningscenter Risœ. Risœ-R (Danmarks Tekniske Universitet, Risø Nationallaboratoriet for Bæredygtig Energi)
[19] Aagaard Madsen H, Bak C, Schmidt Paulsen U, Gaunaa M, Fuglsang P, Romblad J, Olesen N, Enevoldsen P, Laursen J and Jensen L 2010 *The DAN-AERO MW Experiments* Denmark. Forskningscenter Risø. Risø-R (Danmarks Tekniske Universitet, Risø Nationallaboratoriet for Bæredygtig Energi)
[20] Jonkman J, Butterfield S, Musial W and Scott G 2009 Definition of a 5-MW Reference Wind Turbine for Offshore System Development URL `http://www.nrel.gov/wind/pdfs/38060.pdf`
[21] Mikkelsen R, Sørensen J and Troldborg N 2007 Prescribed wind shear modelling with the actuator line technique *EWEC*
[22] Troldborg N, Sørensen J N, Mikkelsen R and Sørensen N N 2014 A simple atmospheric boundary layer model applied to large eddy simulations of wind turbine wakes *Wind Energy* **17**
[23] Sarlak H, Mikkelsen R and Sørensen J 2015 Comparing wall modeled LES and prescribed boundary layer approach in infinite wind farm simulations *Proc. of 33rd Wind Energy Symposium* (AIAA)
[24] Mann J 1998 Wind field simulation *Probabilistic Engineering Mechanics* **13** 269–282 ISSN 0266-8920
[25] Jensen N O 1983 A note on wind generator interaction
[26] Frandsen S, Barthelmie R, Pryor S, Rathmann O, Larsen S, Højstrup J and Thøgersen M 2006 Analytical modelling of wind speed deficit in large offshore wind farms *Wind Energy* **9** 39–53
[27] Andersen S J, Sørensen J N, Ivanell S and Mikkelsen R F 2014 Comparison of Engineering Wake Models with CFD Simulations *J. Phys.: Conf. Ser.* **524** 012161
[28] Simley E, Pao L Y, Gebraad P and Churchfield M 2014 Investigation of the Impact of the Upstream Induction Zone on LIDAR Measurement Accuracy for Wind Turbine Control Applications using Large-Eddy Simulation *J. Phys.: Conf. Ser.* **524** 012003
[29] Sescu A and Meneveau C 2014 A control algorithm for statistically stationary large-eddy simulations of thermally stratified boundary layers *Quart. J. R. Met. Soc.* **140** 2017–2022